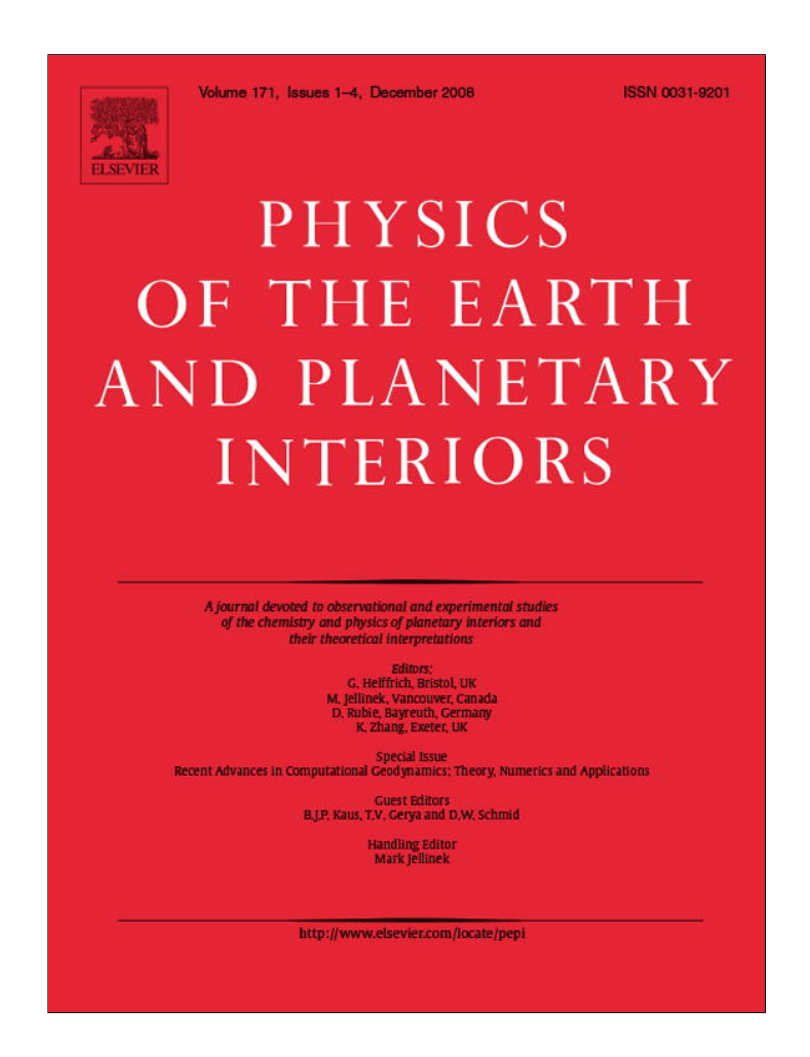
Provided for non-commercial research and education use. Not for reproduction, distribution or commercial use.



This article appeared in a journal published by Elsevier. The attached copy is furnished to the author for internal non-commercial research and education use, including for instruction at the authors institution and sharing with colleagues.

Other uses, including reproduction and distribution, or selling or licensing copies, or posting to personal, institutional or third party websites are prohibited.

In most cases authors are permitted to post their version of the article (e.g. in Word or Tex form) to their personal website or institutional repository. Authors requiring further information regarding Elsevier's archiving and manuscript policies are encouraged to visit:

http://www.elsevier.com/copyright

# **Author's personal copy**

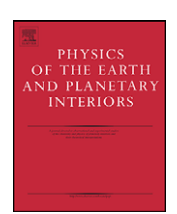
Physics of the Earth and Planetary Interiors 171 (2008) 265-279



Contents lists available at ScienceDirect

# Physics of the Earth and Planetary Interiors

journal homepage: www.elsevier.com/locate/pepi



# Episodicity in back-arc tectonic regimes

Stuart R. Clark<sup>a,\*</sup>, Dave Stegman<sup>b</sup>, R. Dietmar Müller<sup>a</sup>

- <sup>a</sup> Earthbyte Group, School of Geosciences, University of Sydney, NSW 2006, Australia
- <sup>b</sup> School of Mathematical Sciences and Monash Cluster Computing Centre, Monash University, Clayton, Victoria, Australia

### ARTICLE INFO

Article history: Received 31 October 2007 Received in revised form 19 March 2008 Accepted 25 April 2008

Keywords: Subduction Back-arc extension Episodicity Slab rollback Hinge-migration Fluid dynamic modelling Sea-floor spreading

### ABSTRACT

The evolution of back-arc basins is tied to the development of the dynamics of the subduction system they are a part of. We present a study of back-arc basins and model their development by implementing 3D time-dependant computer models of subduction including an overriding plate. We define three types of episodicity: pseudo-, quasi- and hyper-episodicity, and find evidence of these in nature. Observations of back-arc basin ages, histories of spreading, quiescence and compression in the overriding plate give us an understanding of the time-development of these subduction zones and back-arc basins.

Across the globe today, a number of trenches are advancing—the Izu-Bonin Trench, the Mariana Trench, the Japan Trench, the Java-Sunda Trench and the central portion of the Peru-Chile Trench (the Andes subduction zone). The Izu-Bonin, Mariana and Japan all have established back-arc basins, while the others have documented episodes of spreading, quiescence, compression or a combination of these. The combination of advancing and retreating trench motion places these subduction zones in the category of hyper-episodicity.

Quasi-episodicity, in which the back-arc shifts between phases of rifting, spreading and quiescence, is the dominant form of episodic back-arc development in the present. We find this type of episodicity in models for which the system is dynamically consistent—that we have allowed the subducting plate's velocity to be determined by the sinking slabs' buoyancy. Quasi- and hyper-episodicity are only found in subduction zones with relatively high subducting plate velocities, between 6 and 9 cm/year. Finally, those subduction zones for which the subducting plate is moving slowly, such as in the Mediterranean or the Scotia Sea, experience only pseudo-episodicity, where the spreading moves linearly towards the trench but often does so in discrete ridge-jump events.

© 2008 Elsevier B.V. All rights reserved.

## 1. Introduction

The development and evolution of back-arc basins represents a fundamental process of plate tectonics, many aspects of which remain unexplained. Part of the enigmatic nature of back-arc basins is that while they form at convergent plate boundaries, they represent extensional processes which are opposite to the sense of convergence. Even after extensional stresses generated from trench rollback (and retrograde migration of their associated slabs) were identified as the likely origin of back-arc basins (Dvorkin et al., 1993; Faccenna et al., 1996; Jolivet et al., 1994), the exact mechanism as to how subduction dynamics controlled the process was not apparent. Thus, the problem of back-arc basin formation serves as a clear indicator that our understanding of subduction remains inadequate.

E-mail address: stuart@simula.no (S.R. Clark).

Some insight can be gained into these processes by considering the kinematics associated with back-arc basins, which reflect the product of relative motions between the trench, the subducting plate and the overriding plate. A large amount of episodicity can be seen in the recent kinematic synthesis of Sdrolias and Müller (2006), which reports the evolution of back-arc basins in the Pacific ocean during the past 60 Ma. The distribution of sea-floor age suggests extension alternating with phases of tectonic quiescence or compression. Similar arguments can be made for observations related to orogenesis, that the state of mountain building is determined by the trench velocity, and whether it is advancing towards the overriding plate or retreating from it (Lister et al., 2001).

Recent global compilations of the trench motion demonstrate that between 50% and 75% of trenches (depending on choice of absolute reference frame) are currently retreating (Lallemand et al., 2005; Schellart et al., 2007). The remaining trenches are either neutral or advancing, and in the Indo-Atlantic hotspot reference frame there are only a few trenches advancing at present: Japan (1.5 cm/year), Izu-Bonin (2.65 cm/year), Mariana (1.85 cm/year), Sunda (0.7 cm/year), Hikurangi (2.1 cm/year) and

<sup>\*</sup> Corresponding author. Current address: Computational Geosciences, CBC, Simula Research Laboratory, Martin Linges v. 17, Snarøya, 1367, Norway. Fax: +47 67828201.

Bolivia (0.5 cm/year) (Schellart et al., 2007). However, the static view for the present day can be misleading with regards to the motion of trenches because although plate motions may generally be considered smooth and continuous, the motion of plate boundaries is not.

There are other processes besides trench motion which are important in producing back-arc basins, but may also greatly influence the episodicity of basins. Extensional forces may arise from gravitational collapse of regions with thickened crust (Martinod et al., 2000) or from far-field stresses due to changes in plate direction and continent–continent collisions (Silver et al., 1998). These effects have been shown to be important for back-arc basin development in the Aegean and Japan Seas as their contribution likely modulated the more dominant extensional forces from roll-back subduction (Jolivet et al., 1994).

One well-documented case of back-arc basin evolution is that of the Central Mediterranean (Faccenna et al., 2001 and references therein). There, two episodes of extension have occurred since 30 Ma, each beginning with slow rifting and punctuated with fast back-arc spreading. The Liguro-Provençal basin was formed by thinning and rifting for  $\sim\!8\,\text{Myr}$  between 30 and 22 Ma, followed by  $\sim$ 6 Myr of oceanic spreading between 22 and 15 Ma. There is then an apparent 5 Myr hiatus in extension while the ridge jumps to the southeast from 16 to 10 Ma. Extension then resumes for a 5 Myr period of rifting and subsidence, forming the Tyrrhenian basin, followed by new spreading centres within the basin active from 5 Ma to present. These two spreading centres show a linear progression towards the retreating trench (Faccenna et al., 2001; Spadini and Podladchikov, 1996). We classify this as pseudo-episodicity as the overriding plate rheology leads to distinct phases of back-arc spreading although the trench motion is in constant retreat.

The best examples for studying the development of back-arc basin are the large intra-oceanic basins of the Western Pacific. These include the Shikoku, Perace Vela, West Phillipine, Lau, North-Fiji and South Fiji Basins, the Japan, South China and Sulu Seas, as well as the Marianas Trough. We use revised interpretations and compilations of the history of seafloor spreading (Müller et al., 2006) in these regions, as well as a few regions outside the Western Pacific, for example the Scotia Sea. These are combined with recent observations in other nearby marginal basins which together form an ensemble of basins associated with an individual subduction zone. The pattern which emerges from such a synthesis may then be placed into context with the regional dynamics as they are controlled by subduction processes. This regional view of back-arc basin evolution applied worldwide can provide a framework for distinguishing between different types of observed episodicity.

There is a variety of episodicity exhibited in regions with backarc basins which ultimately reflect the evolution of the stress field. In some cases, extension may be continuously ongoing but an apparent hiatus in extension is either due to a lack of data or a ridge-jump followed by a period of rifting preceding extension, such as the case in the Mediterranean. Either of these cases we term pseudo-episodic. Otherwise, episodic behaviour is observed when extension is interrupted by periods of quiescence (i.e. an actual hiatus of extension) or compression, which we term quasi-episodic and hyper-episodic, respectively.

Various approaches have been adopted for investigating how subduction influences the stress field in the overriding plate. Compilations of subduction related parameters and relevant geologic observations in the overriding plate have been made with the goal to classify tectonic regimes and identify correlations (Heuret and Lallemand, 2005; Jarrad, 1986; Lallemand et al., 2005; Whittaker et al., 2007). Attempts to quantitatively understand how particular parameters affect the dynamics of subduction systems are largely based on analogue and numerical models, however, the full com-

plexity of subduction is difficult to address. Consequently, models typically introduce one or more simplifications such as restricting the dynamics to a 2D geometry, not including an overriding plate or including an overriding plate but in the absence of any interaction with the fluid mantle. Furthermore, many models are not dynamically self-consistent because conditions such as plate speed, trench location or dip angle have been prescribed a priori.

Much of the attention spent on understanding subductiondriven dynamics of the overriding plate has been focused upon the use of 2D numerical models (Buiter et al., 2001; Sobolev and Babeyko, 2005). However, in regard to back-arc basins, the motion of the trench is of primary importance in controlling the time-dependent stress field in the region of the plate boundary. Unfortunately, most 2D models do not achieve self-consistent trench motion because in order to produce one-sided subduction, either the trench location, trench motion or plate motion are prescribed. Models of free subduction are preferable because they treat trench and plate kinematics as emergent features completely driven by the negative buoyancy of the subducting slab (Enns et al., 2005; Funiciello et al., 2003b; Garfunkel et al., 1986). However, one of the limiting factors in models of free subduction has been to include an overriding plate, a plate that interacts strongly with the subducting slab.

Because subduction zones have a finite lateral extent, the mantle flow induced by subducting slabs and the associated subduction dynamics is inherently three-dimensional. A number of analogue and numerical studies have demonstrated that 3D geometry is essential in order to allow mantle flow around slab edges and generate rollback subduction (Dvorkin et al., 1993; Funiciello et al., 2003a; Garfunkel et al., 1986; Schellart, 2004). It was postulated and shown analytically that the corner flow of 2D numerical models is only applicable to 3D models if subducting slabs are sufficiently wide (Dvorkin et al., 1993).

Such wide slabs (infinitely wide in 2D) prevent mantle flow around the edges of the subducting slab, and the entire mantle flow is forced around the tip of the slab. This reduces the ability of the mantle to flow from underneath the slab to the top of the slab, leading to a difference in pressure and a consequent hydrodynamic lift force that supports the slab the slab and inhibits rollback. The mantle flow around the edges of narrow slabs significantly reduces the pressure exerted on the slab, and this reduction is entirely dependent on the finite extent of the slab. The reduced corner suction allows the weight of the slab to exceed the strength of the subducting plate (i.e. the plastic yield stress limit integrated over the plate thickness). This drives an instability expressed as retrograde hinge migration (rollback) in narrow slabs which has been attributed to the origin of back-arc basins and back-arc spreading in the overriding plate (Dvorkin et al., 1993).

This effect is seen quite dramatically in fully dynamic models when the lateral extent of the subducting plate is varied for the full range of plate widths (300–7000 km) that occur on Earth and plate width is a controlling factor for how trenches move and evolve with time (Schellart et al., 2007). Much of the recent work in 3D has been focused on investigating dynamics of a subducting plate and its associated mantle flow in the absence of any overriding plate (Bellahsen et al., 2005; Funiciello et al., 2003a; Morra et al., 2006; Schellart, 2004; Stegman et al., 2006). However, some studies account for the effect of density perturbations due to ridges and plateaus on the subducting plate (Martinod et al., 2005; Royden and Husson, 2006).

Early analogue experiments demonstrated that extension in the overriding plate is a direct consequence of retrograde slab migration (Kincaid and Olson, 1987). Although these models used a free subduction approach which incorporated an overriding plate, no systematic or quantitative investigation of the dynamics of the

overriding plate was made. Deformation in the overriding plate that is driven by the interaction of a subducting slab has been investigated with 3D models in more detail than these early analogue experiments. However, one limitation of these models is that either the convergence rates are prescribed using pistons (Regard et al., 2005, 2003; Shemenda, 1993; Shemenda and Groholsky, 1994) and are therefore not dynamically self-consistent, or that these models do not incorporate the effect of the underlying mantle flow and are not fully coupled systems as a result.

These recent models largely focus on 3D aspects of convergence such as oblique subduction, continental collision subsequent to the closure of a small ocean between two continents with an equal lateral extent, or collision between a smaller continental mass indenting into a larger continent (Regard et al., 2005). The systematic investigation of how subducting plates influence oceanic overriding plates remains relatively unaddressed. This paper provides a methodology for including an overriding plate in 3D models.

The state of stress in the overriding plate is the product of the delicate balance of large tectonic forces in a highly coupled system, and must therefore include all components of the system: the subducting plate, the overriding plate, and the underlying mantle flow which couples everything together. Furthermore, in order for the resultant dynamics and motion of the trench to be self-consistent, the system must be primarily driven by the slab buoyancy and as much of the remaining problem should be left as little prescribed as possible.

In an attempt to understand the basic dynamics of the system, we have neglected thermo-mechanical effects, which are important on longer time-scales. We have previously looked at these effects in the context of models with imposed kinematic and thermal histories (Clark and Müller, in press), but in this paper we seek to simplify the physics of the development of back-arc basins by considering only the buoyancy and rheological effects of temperature as a first step in understanding back-arc basin time-dependent evolution.

We focus our attention on the episodicity of deformation in the overriding plate by examining 3D models of free subduction incorporating an oceanic overriding plate. We examine how this episodicity is affected through interaction with a subducting slab, either driven by its own negative buoyancy alone or in combination with a surface velocity boundary condition imposed on the subducting plate.

#### 2. Numerical model

A numerical model is advanced which builds on previous work including an overriding plate, a weak zone to reduce the coupling between the subducting and upper plates, and a 3D solver. We setup 14 models with varying width, overriding plate spreading centre and boundary conditions.

#### 2.1. Model setup

We model the subduction system as a subducting plate sinking underneath an overriding plate. The subducting plate (and its associated slab) is a composite material with a visco-plastic upper-half and a purely viscous lower-half (Fig. 1b). The upper layer in these models thus represents the brittle portion of the oceanic lithosphere, as well as a relatively weak serpentinised layer (Lee and Chen, 2007) while the lower portion of the oceanic lithosphere is composed by strong, mantle residuum. This lower layer of the lithosphere can also be thought of as containing the viscous equivalent of a strong elastic core (Morra and Regenauer-Lieb, 2006).

Incorporating a lower layer that cannot yield, results in a strong coupling between the subducted slab and the trailing plate. This

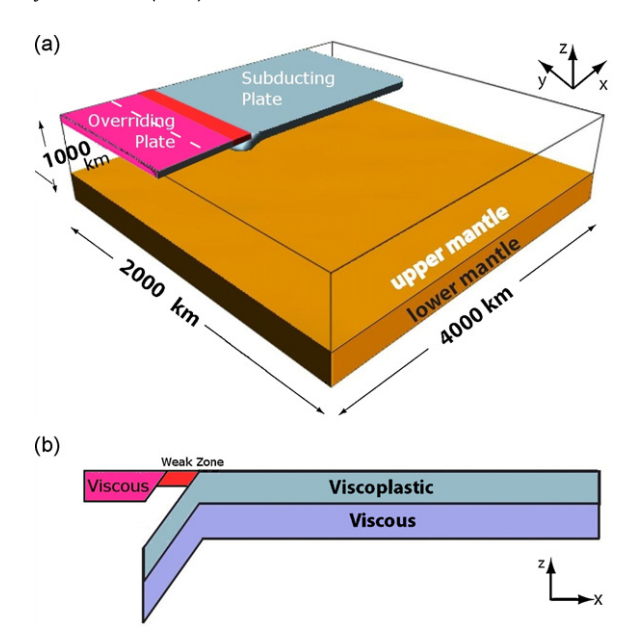


**Fig. 1.** Initial model setup, showing the overriding plate in pink, the island arc material in red and the subducting plate in grey-blue (visco-plastic top layer) and purple (viscous lower layer). (a) 3D representation of the setup showing the region of computation. The upper mantle is transparent and goes to 670 km depth, while the lower mantle is only included until 1000 km depth and is displayed in orange. The dashed line indicates the location of the ridge included in some models. (b) A cross-sectional representation of the two plates and island arc (weak zone). See text for a discussion of the relative sizes.

coupling allows a significant slab pull through the plate's hinge (Schellart et al., 2007). The strength parameters for these layers are presented in Table 1 with the weak upper layer having subscript pl. The initial viscosity is 200 times that of the upper mantle throughout the slab. Plate thickness is kept constant at 100 km, representing mature oceanic lithosphere, but we consider variations in plate-width between 600, 1200, or 2000 km.

Subduction is initiated with a  $500\,\mathrm{km}$  long perturbation at a  $60^\circ$  angle from the surface, which allows us to explore subduction dynamics without having to consider the complexities of subduction initiation. The perturbation is larger than in similar models without an overriding plate as the resistance to establishing subduction is higher. The experiments are conducted in a box which is  $4000\,\mathrm{km}$  long,  $1000\,\mathrm{km}$  deep and  $4000\,\mathrm{km}$  wide, however the symmetry of the problem allows us to divide the computational domain across the middle of the slab so only  $2000\,\mathrm{km}$  of the box width is modelled (Fig. 1a).

The lower mantle begins at 660 km depth and is represented by a sharp interface and viscosity contrast of 100 times the vis-

**Table 1** Model parameters

$\eta_{\mathrm{um}}$ , reference viscosity (upper mantle)	$1\times 10^{20}Pas$
$\Delta \rho$ , density contrast	$80  \text{kg m}^{-3}$
g, acceleration due to gravity	$10  \mathrm{m  s^{-2}}$
H, plate thickness	100 km
L, box depth	1000 km
Depth to lower mantle	660 km
$\eta_{\rm lm}/\eta_{\rm um}$ , lower/upper mantle viscosity contrast	100×
$\eta_{\rm pl}/\eta_{\rm um}$ , lithosphere/upper mantle viscosity contrast	200×
$ au_{ m ref}$	800 MPa
$ au_{ m pl}$	48 MPa
$\mu_{ m pl}$	0.1
$ au_{ m arc}$	4 MPa
$\mu_{ m arc}$	0.2
Imposed plate velocity (where present)	7.0 cm/year

cosity of the upper mantle. While lower contrasts have been used in previous studies (Bunge et al., 1997; Christensen, 1996; Forte and Peltier, 1991), we have neglected the retarding effect of the clapeyron slope on the buoyancy of the slab and therefore seek to compensate through a higher viscosity contrast. A stratified mantle viscosity is essential for both confining slab dynamics and induced mantle flow to the upper mantle, as well as anchoring slabs which have penetrated into the more viscous lower mantle (Funiciello et al., 2003a; Gurnis et al., 2000; Han and Gurnis, 1999; Zhong and Gurnis, 1995a,b).

The model resolution is 50 km in the trench parallel and trench perpendicular directions, and 25 km in the vertical direction. In particular high resolution in the vertical direction is required to properly resolve the lithosphere and exceeds that previously used in buoyancy-driven models (Schellart et al., 2007; Stegman et al., 2006). Resolution tests have also been performed by Stegman et al. (2006).

The overriding plate thickness is kept constant at 50 km, representing relatively young lithosphere, while its width is the same as that of the subducting plate. However, the overriding plate is comprised only of a purely viscous layer, ignoring stress dependent effects, in contrast to the two-layered rheology of the subducting plate. The trailing edge of the overriding plate is attached to the wall with a no-slip condition and the plate is 1390 km long.

A-300 km wide 'side plate', with the same composition as the overriding plate, is attached to the side of both the overriding plate and the subducting plate. This side plate is introduced to represent a closer approximation to the real world in which the subducting plate system is not isolated but linked to a surface wholly comprised of plates.

Between the overriding plate and the subducting plate, a very weak and buoyant material (we will use the terms 'weak zone' and 'island arc' for this material interchangeably) is introduced which prevents the overriding plate from becoming entrained and facilitates one-sided subduction. This material represents chemically buoyant continental crust, as well as partially molten material rising off the slab. This material has lower density than that of the upper mantle by  $320\,\mathrm{kg/m^3}$  and is 10 times less viscous than the overriding plate. To promote decoupling between the overriding and subducting plates (in lieu of a plate bounding fault), the cohesive strength is reduced to only 4 MPa.

Geometrically, this material is ascribed by a trapezoidal prism, whose cross-section is 110 km across at the surface, follows the slab down to a depth of 25 km and then turns back towards the overriding plate until it ascends vertically back to the surface. This shape was chosen experimentally as a narrower weak region led to entrainment of the overriding plate with the downgoing slab, while a less buoyant material disappeared through subduction

To test the influence on the mantle dynamics of the presence of young oceanic lithosphere, adjacent to a back-arc spreading centre in the overriding plate, a weak zone is included in the middle of the overriding plate. In contrast to island arc material, this material is continuous with the upper mantle and cuts a trapezoidal prism out of the overriding plate. We denote models of this type with an 'R' suffix if a ridge is present. A cross-section of the trapezoidal prism has a short side on the surface 100 km wide and a long side at the base of the overriding plate and 310 km wide and is vertically symmetrical. The prism runs parallel to the trench for the entire length of the overriding plate and is 880 km from the edge of the box (Fig. 1).

Examining the boundary conditions interplay with the dynamics of the overriding plate is our focus in this paper. Incoming plate age and overriding plate motion have not been tested in our models as Sdrolias and Müller (2006) found these variables only impor-

tant in the initialisation of back-arc spreading, not in its continuous development.

#### 2.2. Governing equations

We treat the problem as an isothermal Rayleigh–Taylor instability problem by assigning appropriate density variations arising from temperature and neglecting thermal diffusion (neither the thickness nor buoyancy of the subducting plate change appreciably over the duration of the experiment). Consequently, ambient mantle has neutral buoyancy while the slab and the overriding plate have a negative buoyancy force due to the density variation used above.

Considering the sum of forces on any given body of fluid must be zero, the forces due to pressure, deviatoric stress and gravity must balance. The deviatoric stress tensor is given by the equation:

$$\tau_{ij} = \eta \left( \frac{\partial u_i}{\partial x_j} + \frac{\partial u_j}{\partial x_i} \right) \tag{1}$$

where  $\eta$  is the viscosity and u is the velocity. Thus the principle of the conservation of momentum gives the following:

$$-\nabla \vec{p} + \nabla \left( \eta \left( \frac{\partial u_i}{\partial x_j} + \frac{\partial u_j}{\partial x_i} \right) \right) + \Delta \rho g \hat{z} = 0$$
 (2)

where p is the fluid pressure and  $\Delta \rho g \hat{z}$  is the buoyancy of the material due to the viscosity contrast,  $\Delta \rho$ , multiplied by the force due to gravity, g, and applied only in the vertical direction, by multiplying by a unit vector pointing in the vertical direction. We use the approximation that the fluid is incompressible and therefore within any given volume the divergence of the velocity field must be zero.

$$\nabla \cdot \vec{u} = 0 \tag{3}$$

Finally, we allow yielding of the weak zone and the upper-layer of the subducting plate according to Byerlee's method in which the viscosity of the material is reduced by a function of the second invariant of the deviatoric stress, if the stress at depth z, exceeds the yield strength,  $\tau_y$ , defined in the following equation:

$$\tau_{y} = \tau_{0} + \mu_{0} g \rho z \tag{4}$$

where  $\tau_0$  is the strength of the material at the surface (where z = 0) and  $\mu_0$  is the dimensionless depth-coefficient. This yielding formulation follows the argument of Stegman et al. (2006).

# 2.3. Numerical method

The equations are solved with a combination of Lagrangian and Eulerian methods, with particles advected through a finite element Eulerian mesh (Moresi et al., 2003). As the fluid is incompressible, the Uzawa conjugate gradient method is used to reduce  $\nabla \cdot \vec{u}$  to approximately zero.

Velocity is scaled relative to the Rayleigh–Taylor instability, the scaling factor being directly proportional to the pressure exerted by a unit volume of the instability. This pressure is determined by the density contrast,  $\Delta \rho$ , multiplied by the acceleration due to gravity, g, and the thickness of the layer, H. The velocity scaling factor is also inversely proportional to the reference viscosity of the fluid,  $\eta$ , as a measure of the real speed of the fluid (In the formulas below, a dash to the right of a letter is the dimensionless version of the parameter.) The formula scaling the velocity, v, is

$$v = \frac{\Delta \rho g H L}{\eta} v'$$

where v' is the dimensionless velocity, v is the velocity in m s<sup>-1</sup>,  $\Delta \rho$  is the density contrast, H is the reference distance for change in the model, in this case the thickness of the slab. L is a reference length, here the depth of the box and  $\eta$  is a reference viscosity.

Length is simply scaled relative to the depth of the box, *L*, the major length scale for the problem. The scaling is given below:

$$x = Lx'$$

The scaling of time, t can be derived from the combination of the above two formulas for length and velocity, since v = x/t and v' = x'/t'. As such t is

$$t = \frac{\eta}{\Delta \rho gH} t$$

#### 2.4. Stress and velocity boundary conditions

We focus our investigation on the dynamics of the overriding plate and in particular its kinematics and internal deformation. Apart from the variation of width, the models are varied in terms of whether the trailing edge of the subducting plate is fixed to the wall of the box (no-slip), free to move from the wall (free-slip) or pushed with an imposed surface velocity condition of 7 cm/year from the trailing edge to a line 300 km seaward of the trench (free-slip elsewhere). The gap between the trench and the velocity condition allows the trench to move dynamically.

While a series of subducting plate velocities are not tested in this paper, we chose our boundary conditions to capture the variety of behaviour found on Earth. 7 cm/year serves as an approximation for the velocity of the subducting plate in the vast majority of subduction zones plates that are moving between 6 and 9 cm/year. This includes the Pacific plate and its numerous associated subduction zones in the Western Pacific, the Australian plate and the Java-Sunda and New Hebrides Trenches, as well as the Cocos and Nazca plates.

The 'fixed' boundary condition represents the Hellenic and Calabria Trenches, where the subducting plate is the slow moving African plate. The other major series of subduction zones fall into the 'free category', subducting plates without a major ridge push force and that are slow moving: South American plate and the Scotia and Caribbean Trenches; the Antarctica plate and South Shetland trench; the Juan de Fuca plate and the Middle America Trench (Schellart et al., 2007).

In the 'fixed' models, the subducting plate is attached to the box at its trailing edge. This attachment represents the subducting plate being fixed to a continental plate. In the 'free' models however, the edge is separated from the box and is not pushed, representing a

**Table 2** Models run

Model name	Imposed velocity	Trailing edge	Width (km)	Ridge
Reference	7 cm/year	Imposed	1200	No
600	7 cm/year	Imposed	600	No
2000	7 cm/year	Imposed	2000	No
2000R	7 cm/year	Imposed	2000	Yes
1200freeR	N/A	Free	1200	Yes
600freeR	N/A	Free	600	Yes
2000free	N/A	Free	2000	No
2000freeR	N/A	Free	2000	Yes
1200fixed	N/A	Fixed	1200	No
1200fixedR	N/A	Fixed	1200	Yes
600fixed	N/A	Fixed	600	No
600fixedR	N/A	Fixed	600	Yes
2000fixed	N/A	Fixed	2000	No
2000fixedR	N/A	Fixed	2000	Yes

transform fault. Thus, in models with subducting plates that have free edges, the motion of the subducting plate is driven only by slab pull. In the case of the pushed boundary, the subducting plate's motion is driven by both slab pull and the additional ridge push force generated by a mid-oceanic ridge. Strictly speaking, the free edge models we describe do not exist in nature but are somewhat analogous to plates with very slow spreading rates (i.e. the mid-Atlantic) in which the ridge push force does not translate into fast plate velocities such as those seen in the Pacific. Table 2 lists the models run as part of this research.

#### 3. Results

Episodicity of the trench motion in the numerical models is discussed in relation to back-arc seafloor ages and trench motions derived from kinematic plate reconstructions. The results show hyper-episodicity is found only in those models with an imposed velocity boundary conditions. This finding is confirmed by the back-arc basin ages derived from magnetic lineations. Fig. 2 shows the initial state of the reference model and explains the viewports that will be used in Figs. 5–7. Note that the axis of symmetry is marked with a dashed line and the centre of the trench is marked with a dot.

#### 3.1. Subduction models

The time evolution of the normalised overriding plate area for a selection of the models is shown in Fig. 3. The time evolution is limited to extend to 20 Myr before any of the models become unstable and the overriding plate area has been normalised by dividing by the initial plate area. Increasing and decreasing plate areas cor-

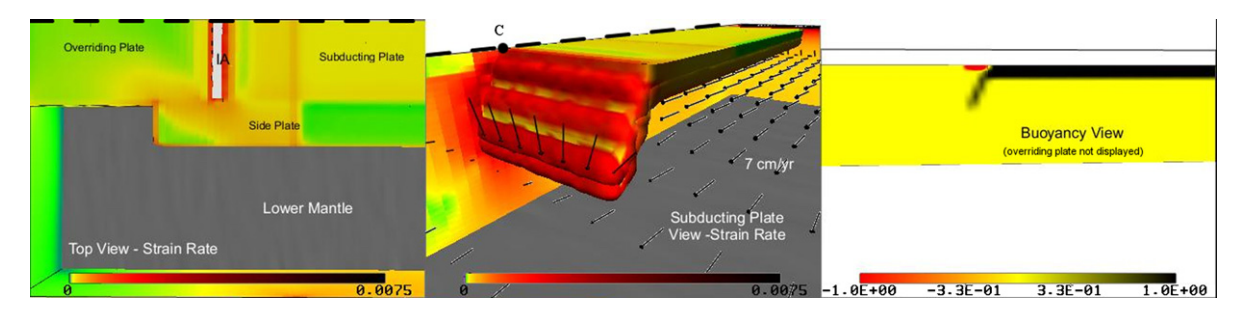


**Fig. 2.** An explanation of the viewports used in Figs. 5–7. The left frame is the dimensionless strain rate from above, including a view of the side plate which is removed for clarity in the other plots. The dashed line in the left and centre frames shows the location of the axis of symmetry. The centre of the trench is marked with a dot labelled C in the centre view. The centre viewport is a perspective view of the dimensionless strain rate, looking only at the subducting plate. Velocity vectors show direction of flow at 200 km depth. The right frame is a view of the cross-section through the middle of the plate (at the boundary of the computational domain) of the dimensionless buoyancy of the subducting plate and the weak zone only (overriding plate removed). The transition zone at 670 km is shown as grey in the left and centre windows and in white in the right cross-section.

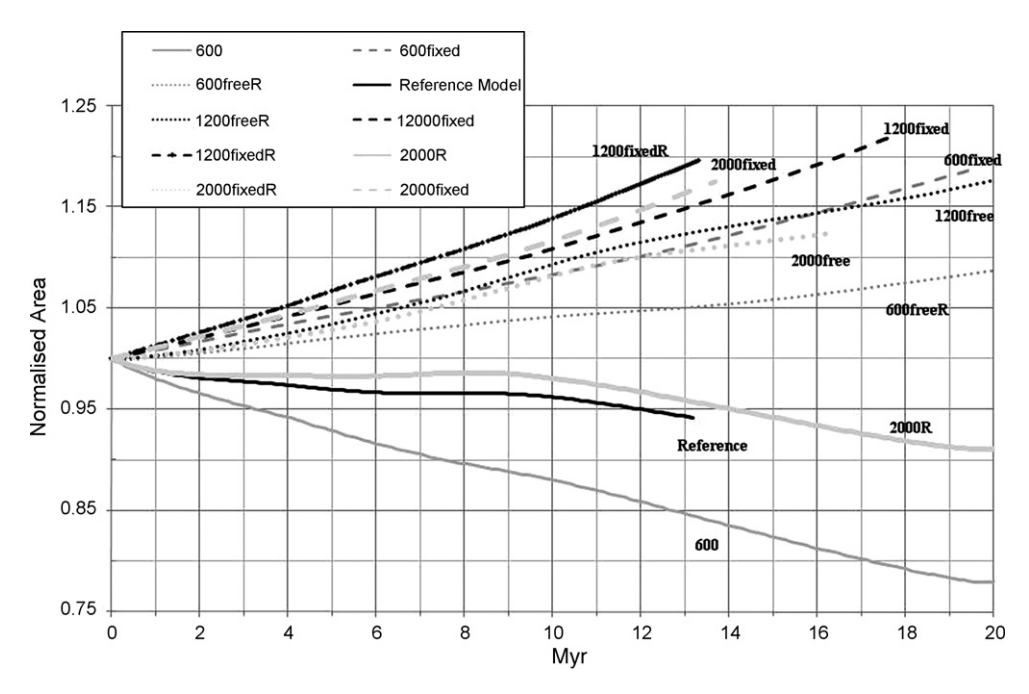


Fig. 3. Normalised area (dimensionless) vs. time (Ma). Dashed lines are the fixed models, dotted lines the free models and solid lines the pushed models. See text for discussion.

respond to extension and compression, respectively. The pushed models (solid lines) are the only models which display a reduction in overriding plate area, having between 77% and 92% of their original area at 20 Myr.

Fixed models have greater relative growth in overriding plate area than their free model counterparts, regardless of width. Adding a ridge to model '1200fixed' increased the overriding plate area from 15% to 20% of the initial area at 13.2 Myr (Fig. 3), while increasing the width of '600fixed' from 600 to 1200 km in model '1200fixed' also led to a 5% increase in the total area at 17 Myr.

'Free' models are grouped below the fixed models regardless of the other parameters involved, following a similar pattern to

the fixed models, with '2000free' following closely the profile of '600fixed' although a little below, while '600freeR' differed by 10% from its counterpart 600fixed' at 19 Myr.

To demonstrate the episodicity in the models, we calculated the trench speed at the edge of the overriding plate for three cases keeping the slab width the same—1200 km (Fig. 4). Each of the three boundary conditions applied to the subducting slab produced three different results. These results are displayed until 14 Myr, long before the subducting plate becomes unstable at between 20 and 25 Myr and collapses wholesale into the mantle. A four-point averaging filter is applied to the results to remove high frequency, low amplitude variations.

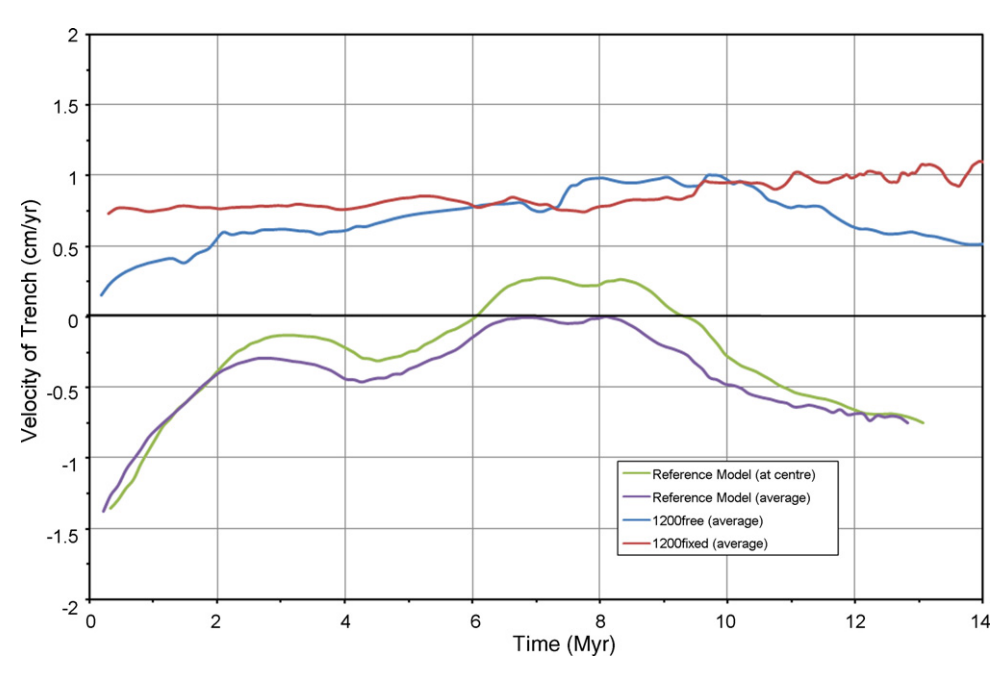


**Fig. 4.** Velocity of the Trench in cm/year plotted against time. The velocities are either calculated at the centre of trench or averaged across 87.5% of the trench, excluding the outermost regions. The trench is taken to be on the boundary of the overriding plate and the weak zone or island arc region. See text for discussion.

# S.R. Clark et al. / Physics of the Earth and Planetary Interiors 171 (2008) 265–279

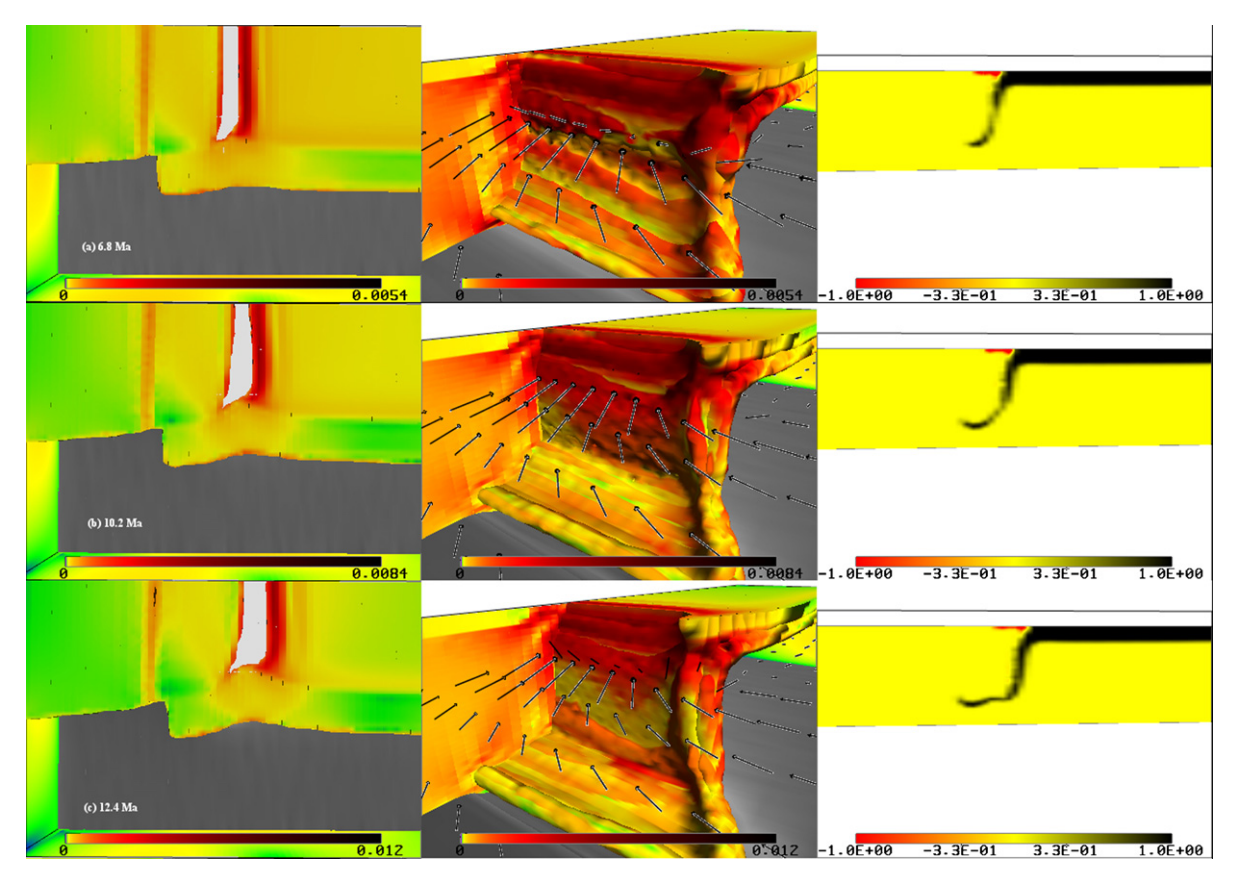
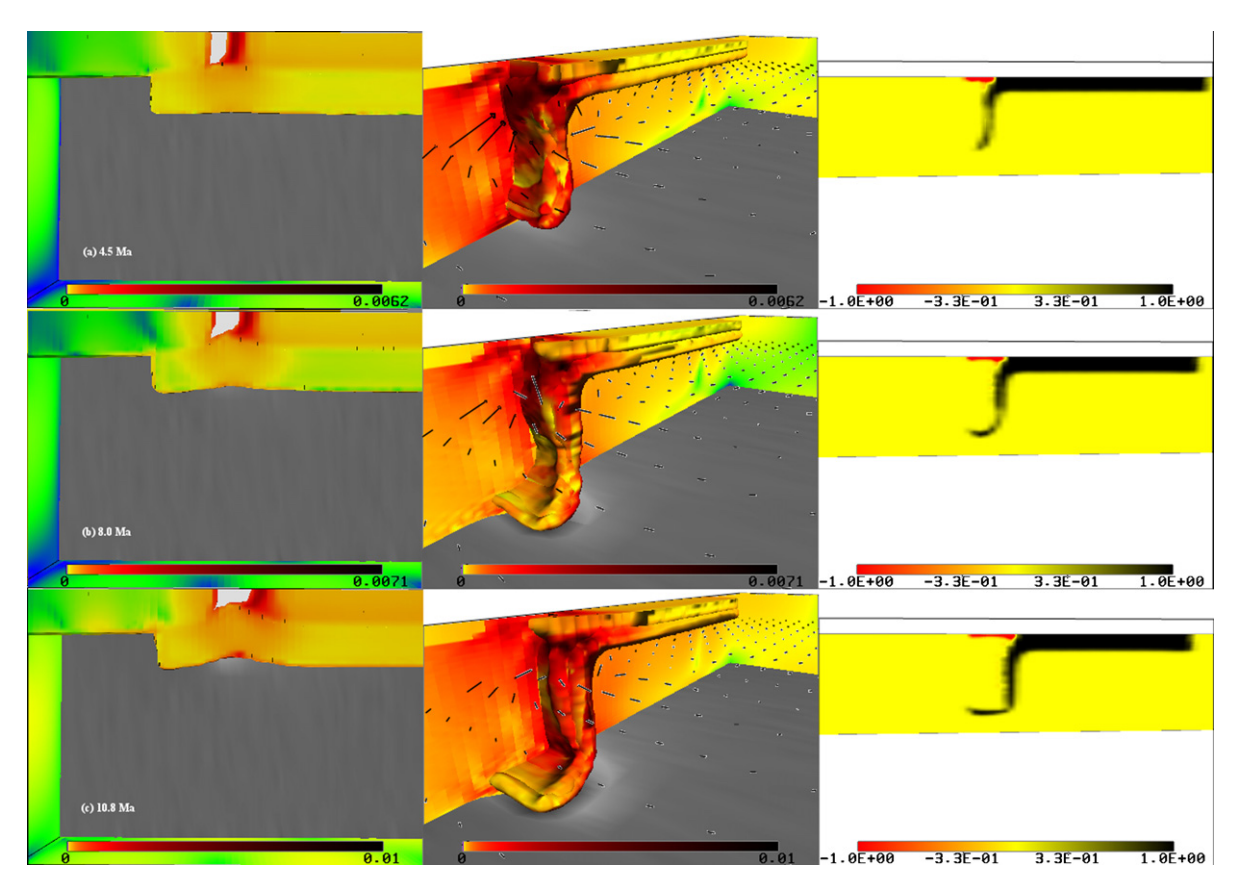


Fig. 5. Snapshots of model '2000fixedR' at (a) 6.8 Myr, (b) 10.2 Myr and (c) 12.4 Myr.



 $\textbf{Fig. 6.} \ \ \text{Snapshots of model '600 free' at (a) 4.5 Myr, (b) 8.0 Myr and (c) 10.8 Myr.}$ 

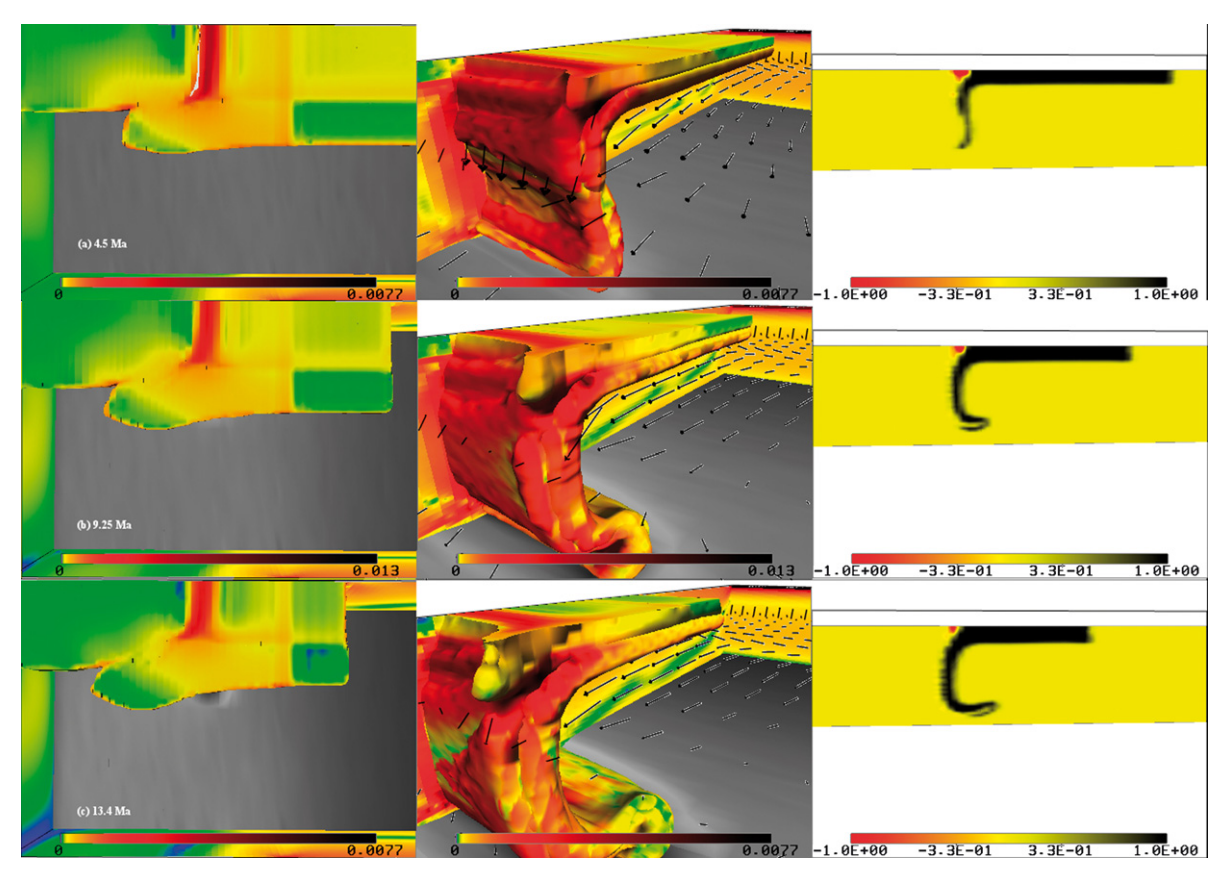


Fig. 7. Snapshots of the reference model at (a) 4.5 Myr, (b) 9.25 Myr and (c) 13.4 Myr.

The 'fixed' model undergoes steady rollback from 0 to 14 Myr, with a rollback speed of  $\sim\!0.75$  cm/year until 8 Myr. Rollback speeds increase from that point to 1.25 cm/year at 11 Myr (Fig. 4). Fig. 5 displays three snapshots of the model 2000fixedR. The trench experiences progressive rollback as is common throughout the series of

fixed models, regardless of width. The fastest rollback occurs initially at the edge of the plate (compare the top views, Fig. 5(a) and (b)) as the mantle flow from under the plate turns around the edge, bending the edge inwards. This bending results in a trench geometry which is strongly concave due to the large lateral variation

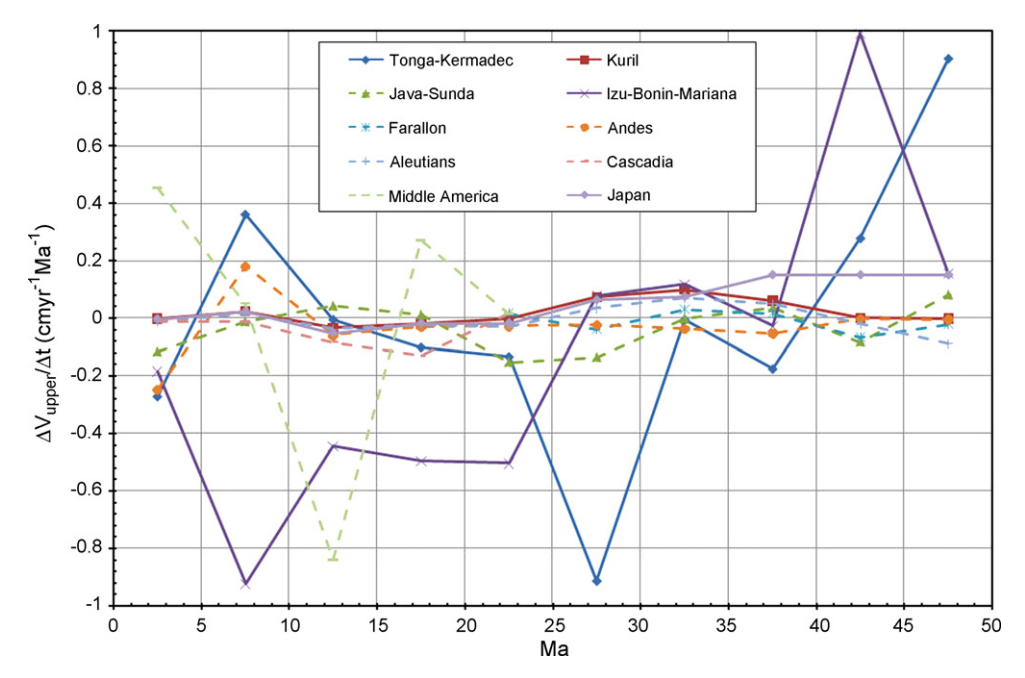
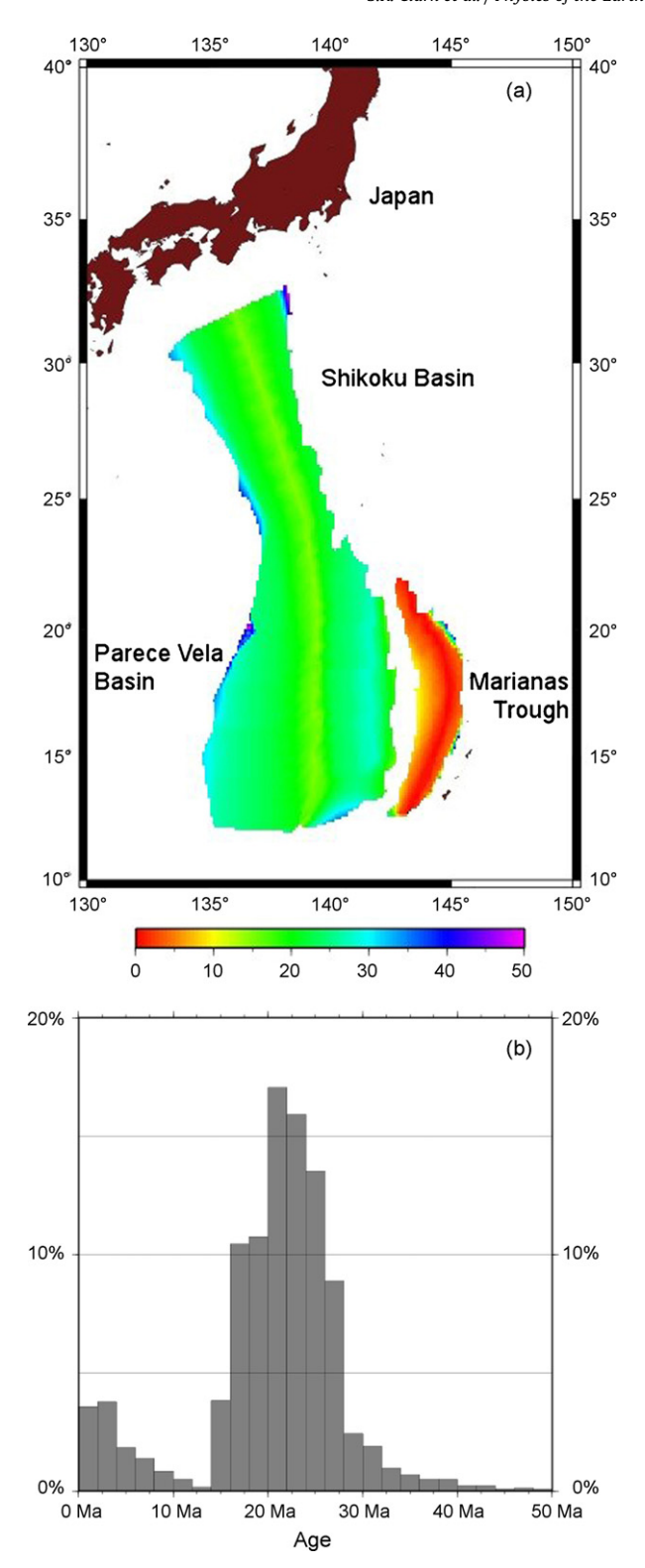


Fig. 8. Derivative of  $v_{upper}$  with respect to time, plotted against time.  $v_{upper}$  is derived from averaging the velocities along trench from Sdrolias and Müller (2006). The velocity along the trench is either the back-arc velocity, in cases in which the back-arc exists, or the overriding plate velocity.



**Fig. 9.** Shikoku Basin, Parece Vale Basin and Marianas Trough ocean floor age represented as: (a) a gridded map and (b) histogram distribution using 2 Myr bin widths.

in trench motion between the sides and centre of the trench. The sinking slab strikes the transition zone at a low angle of incidence, where it bends again to be laid out horizontally as the trench moves backward.

The 'free' model also undergoes only rollback, although rollback speeds increase from almost none (0.2 cm/year) at the start of the

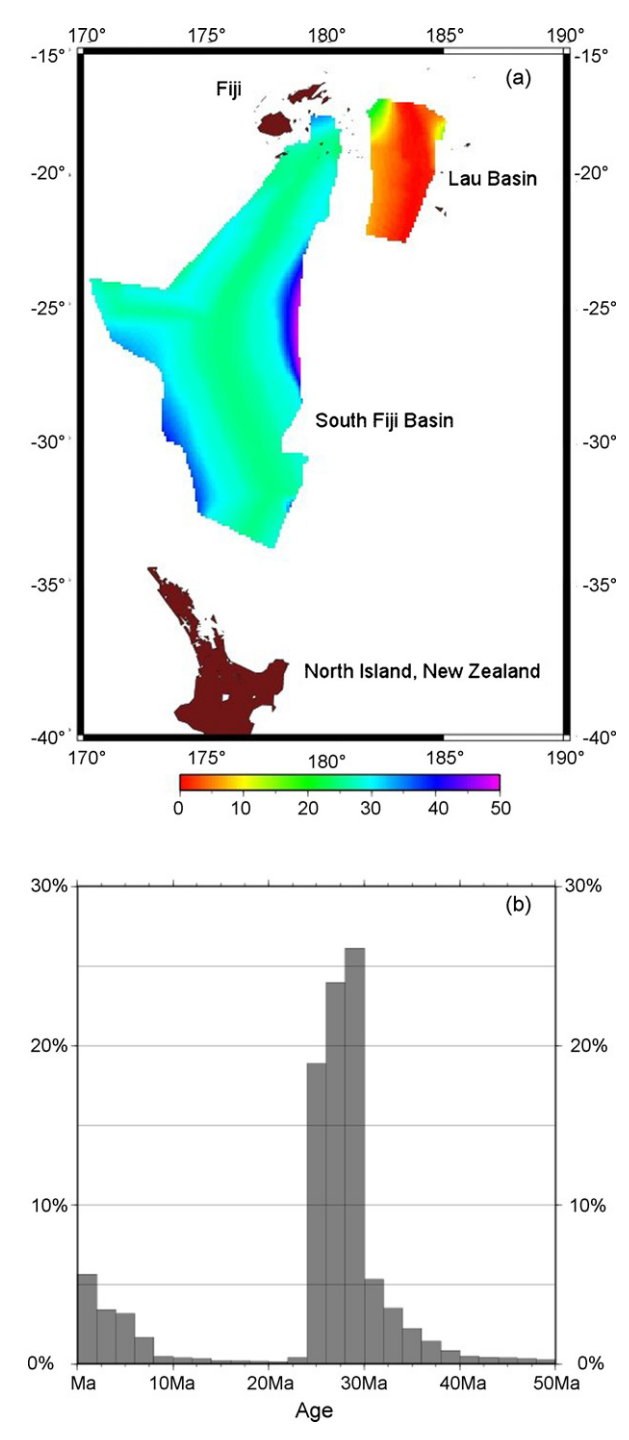


**Fig. 10.** South Fiji Basin and Lau Basin ocean floor age represented as: (a) a gridded map and (b) histogram distribution using 2 Myr bin widths.

model, to 1 cm/year at 8 Myr (Fig. 4). The slab hits transition zone slightly before this causing rollback speeds to gradually decline to 0.5 cm/year at 14 Myr. Fig. 6 shows a narrower free model, model '600free'. Subducting velocities are relatively constant throughout, about 3 cm/year. This slab in the mantle becomes more and more vertical leading to a slowdown in the trench retreat rate.

The subsequent speed up and slow down of the rollback velocity delineates the 'free' models as quasi-episodic from the 'fixed' models. The 'fixed' models are non-episodic in our models, but their parallels in nature may appear episodic, since the particular structure of the overriding plate influences the location of rifting and

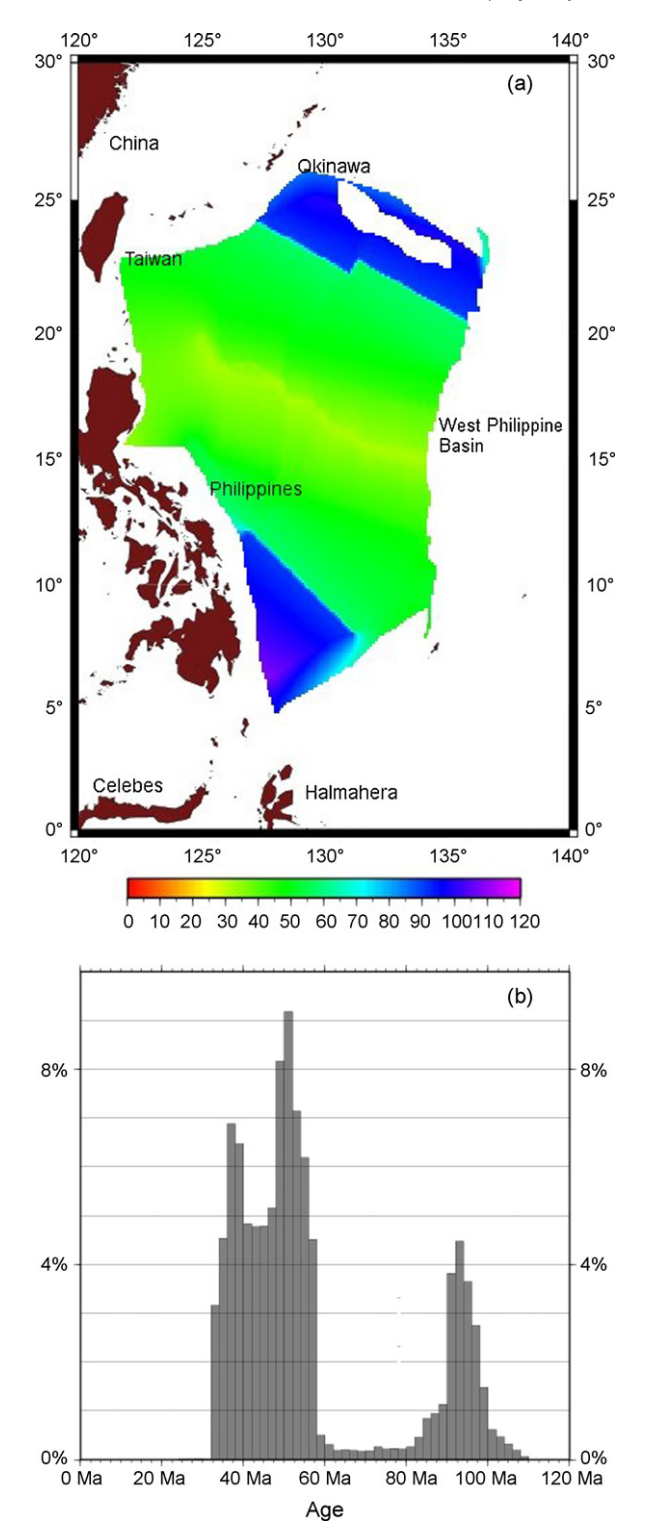


**Fig. 11.** West Philippine Basin ocean floor age represented as: (a) gridded map and (b) histogram distribution using 2 Ma bin widths.

spreading causing ridge-jumps, such as in the Mediterranean. We denote these cases as being pseudo-episodic.

The average trench velocity in the reference model (Fig. 4) is episodic, as trench advance slows from -1.25 cm/year at the start of the model to -0.25 cm/year at 3 Ma. The trench advance then stops between roughly 6 and 8 Myr, before advance continues again to -0.75 cm/year at 13 Myr. Taking a point at the centre of the trench,

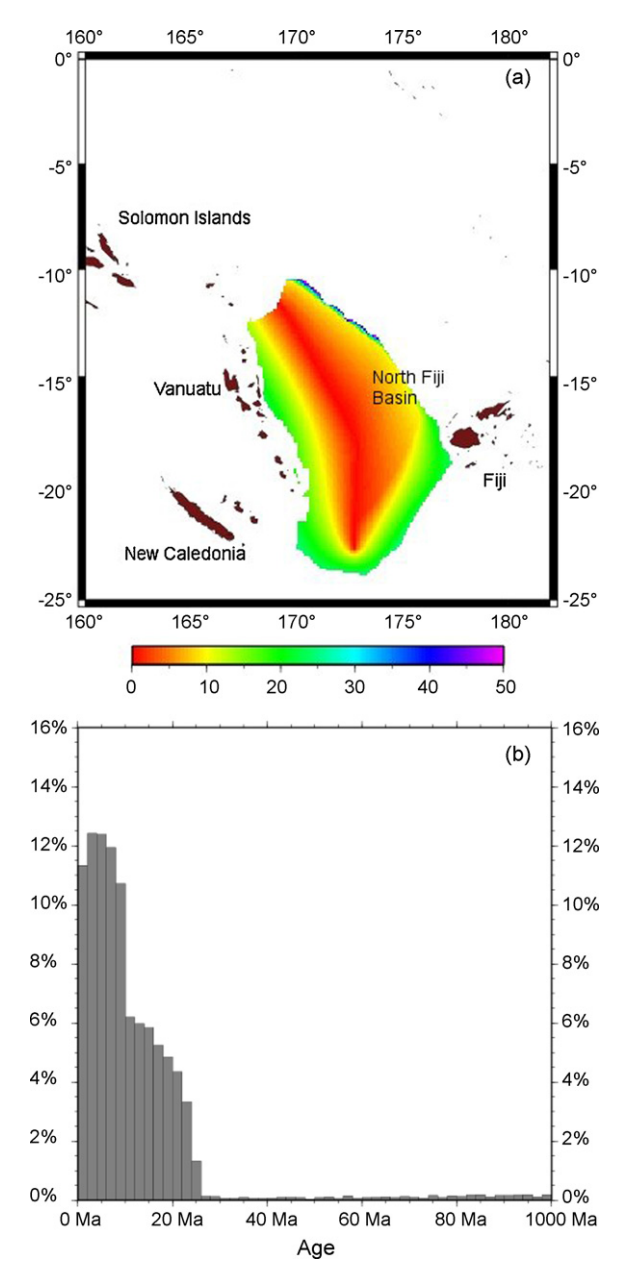


**Fig. 12.** North-Fiji Basin ocean floor age represented as: (a) gridded map and (b) histogram distribution using 2 Ma bin widths.

the episodicity is more evident as rollback actually ensues from 6.1 to 9.2 Myr. This is noticeable in Fig. 7. As parts of the trench experience both trench advance and rollback, the reference model is hyper-episodic.

As an example of hyper-episodicity, three timeframes are shown in Fig. 7 for a pushed slab with a width of  $1200\,\mathrm{km}$  (the reference model) at 4.5, 9.25 and  $13.4\,\mathrm{Myr}$ . The trench position is moving forward in Fig. 7(a), but trench retreat in the centre of the trench is evident when comparing Fig. 7(a) and (b), as is evident from Fig. 4.

# 3.2. Basin age distributions and upper plate velocities

Average upper plate velocities through time are calculated for the Tonga-Kermadec, Java-Sunda, Middle America, Cascadia, Farallon, Kuril, Aluetian, Japan, Andes and Izu-Bonin-Marianas subduction zones based on data in Sdrolias and Müller (2006). Cal-

S.R. Clark et al. / Physics of the Earth and Planetary Interiors 171 (2008) 265–279

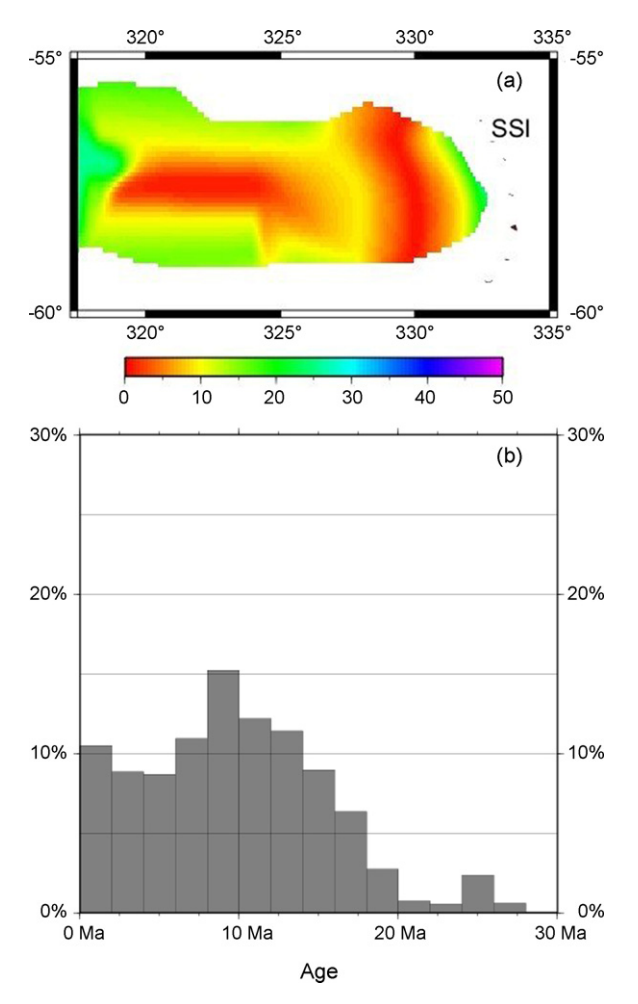


**Fig. 13.** Ocean floor ages in the Scotia Sea represented as: (a) gridded map and (b) histogram distribution using 2 Myr bin widths.

culating the change in velocity between each 5 million time period, we derive the derivative of the average velocity (Fig. 8).

Overriding plates with back-arc basins in Fig. 8 are solid lines, while those without back-arc spreading are dashed. Changes in

velocity are evident in all these cases, with the greatest episodicity in the Tonga-Kermadec, the Izu-Bonin–Mariana and the Cascadia. Those regions with back-arc spreading data more accurately portray the changes in motion of the trench as regions without back-arc spreading do not record any deformation between the trench and the over-riding plate. In all these cases, with the exception of Cascadia, the trench motion undergoes many changes in speed; in all these cases the subducting plate velocity is also high, between 6 and 9 cm/year.

Figs. 9–14(a) show maps of the basin ages of six prominent backarc basins using the oceanic crustal age-grid of Müller et al. (2006). The corresponding histograms of the distributions of ocean floor ages are shown in Figs. 9–14(b) for these basins. Figs. 9–11 show two distinctive sets of seafloor spreading, while Figs. 12–14 show only a single phase of back-arc basin opening.

In Fig. 9, the Marianas Trough opens from 8 Ma (Martinez et al., 1995) after a period of quiescence that followed the opening of the Parece Vale and Shikoku Basins (Sdrolias et al., 2004). In Fig. 10, the South Fiji Basin opening between 35 and 25 Ma (Sdrolias and Müller, 2006) is separated by a nearly 20 Ma gap before the rapid opening of the Lau Basin at 7 Ma (Taylor et al., 1996; Zellmer and Taylor, 2001).

A peak at 92–94 Ma, shown in Fig. 11, contains approximately 4.5% of West Philippine Basin (WPB) ocean floor, representing the first seafloor formed as part of the WPB in the Jurassic-Cretaceous (Deschamps and Lallemand, 2002). Two other phases can be seen, with distinct peaks at 52–54 Ma (9.2% of the WPB) and 34–36 Ma (5.9% of WPB).

In contrast, in Figs. 12–14 the opening of each back-arc is continuous with smooth spreading in the North-Fiji Basin (Fig. 12), Scotia Basin (Fig. 13) and Sulu Sea (Fig. 14). Only a single distribution is seen in the histogram distributions of these seafloor ages in Figs. 12–14(b), respectively.

Opening in the North-Fiji Basin followed the New Hebrides Trench rollback at around 12 Ma (Schellart et al., 2002). Seafloor in Fig. 12 older than this therefore represents remnant seafloor on the edges of the North-Fiji Basin before the polarity of subduction reversed. Since 12 Ma, the amount of seafloor produced has been relatively consistent, with between 10.5% and 12.5% of the current North-Fiji Basin seafloor produced during each 2 Myr period.

The Sulu Sea formed as a back-arc basin in the early Miocene (Silver and Rangin, 1991), shown as a progressively increasing

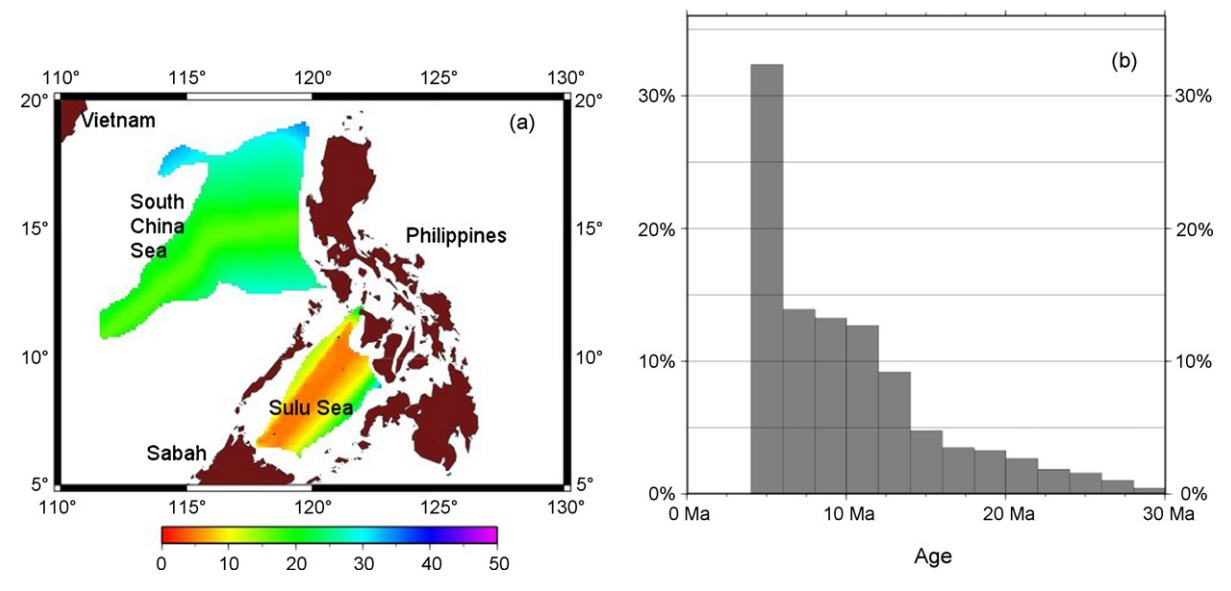
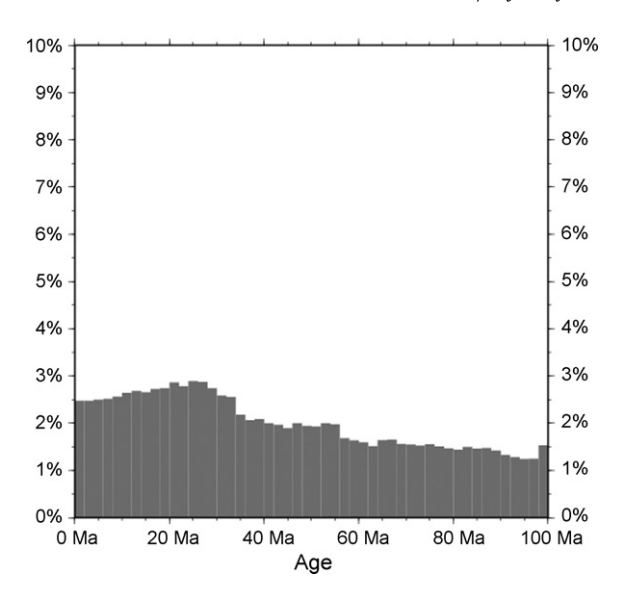


Fig. 14. (a) A gridded map of ocean floor ages in the Sulu and South China Seas and (b) a histogram distribution of sea-floor ages in the Sulu Sea using 2 Ma bin widths.



**Fig. 15.** Ocean floor ages across the world represented as a histogram distribution using 2 Ma bin widths.

proportion of seafloor belonging to younger ages from 30 Ma, reaching a maximum of 32.5% between 2 and 4 Ma, see Fig. 14.

As a comparison, the seafloor age distribution is shown for the entire world in Fig. 15. The world distribution shows a relatively constant distribution of ages, with a higher frequency of younger relative to older ages due to the consumption of older ocean floor due to subduction. In general, the distribution of ocean floor has been fairly uniform, with between 1% and 3% of the current ocean floor ages belonging to each 2 Myr interval (Fig. 15).

In Fig. 16, the back-arc stress regime-compression (dashed), spreading/extension(solid) or quiescence (unmarked)-is shown for the last 45 Ma from the literature presented in Section 1. All of these back-arc regions show episodicity as they move between at least two of these stress regimes. These regions all have incoming subducting plates with high velocities (between 6 and 9

cm/year).

#### 4. Conclusion

Quasi-episodicity is evidenced in Figs. 9–11, in which distinct periods of spreading are separated by quiescence. Both quasi- and hyper-episodicity are seen in Fig. 16. The changing velocities in Fig. 8 highlight that the degrees of episodicity are found in the overriding plate velocities, and hence the trench velocities, particularly when back-arc basin deformation is taken into account.

What these cases have in common is that the subducting plate is moving at a relatively high velocity, 6–9 cm/year, leading to a greater interaction between the overriding plate and the subduction zone. In contrast, for those cases in which the trailing edge of the subducting plates have a lower incoming velocity only pseudo-episodicity is observed (Figs. 12–14) as variations in the overriding plate lead to ridge-jumps as in the case of the Mediterranean and the Scotia Sea. These types of episodicity, derived from observations, correspond to the models of these systems using 3D time-dependant subduction models.

#### 5. Discussion

The evolution of back-arc basins is controlled by the integrated expression of plate kinematics near a subduction zone. This control is inherently time-dependent and three dimensional. However, the plate kinematics can provide a simple conceptual framework for understanding the tectonics of back-arc regions, which can be applied globally to specific subduction systems. From such a generalized framework we gain insight into the underlying dynamics in regards to the nature and origin of observed episodic behaviour.

We introduce a few simple kinematic relations for a general discussion about back-arc tectonics. We define the trench velocity ( $v_{\rm trench}$ ) as positive when the trench is in rollback, following the convention introduced in Section 3 and Fig. 4. The velocity of the subducting plate is then defined as negative quantity to represent motion in the opposite direction. The total rate of convergence ( $v_{\rm subduct}$ ) at the subduction zone, or subduction rate, will then be

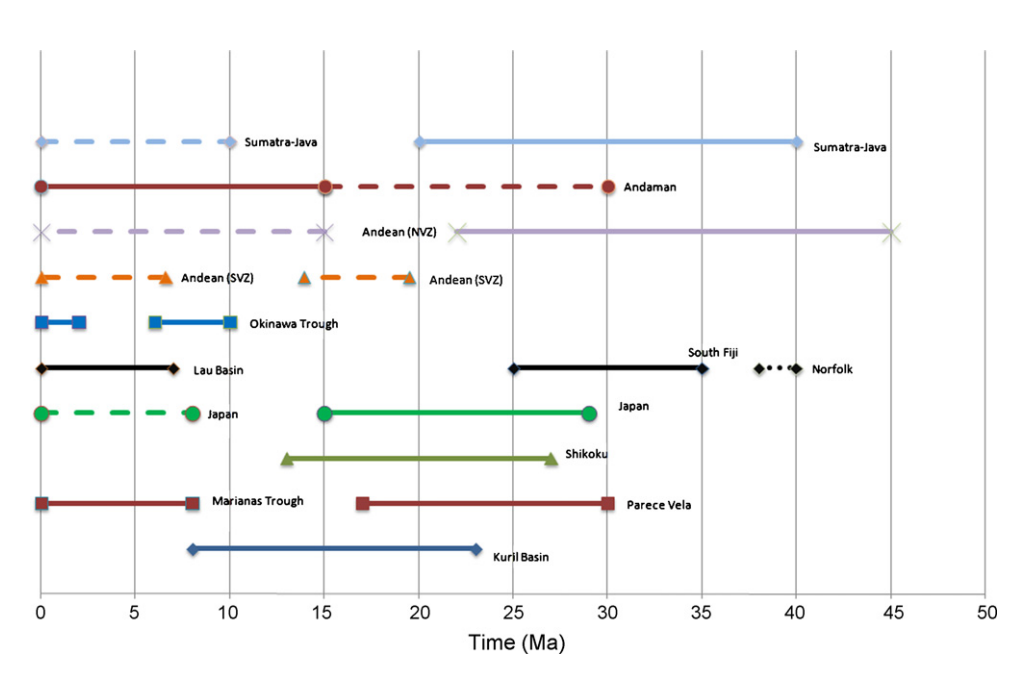


Fig. 16. Back-arc basin tectonics since the middle Eocene. Dashed lines indicate compression, solid lines extension and gaps indicate quiescence.

their difference:

 $v_{subduct} = v_{trench} - v_{plate}$ 

One additional definition required is the motion of the upper plate,  $v_{\rm upper}$ , which we define as positive in the direction of rollback. Kinematically speaking, the entire evolution of back-arc basins can be understood from the time-dependence of just these two quantities: trench motion and upper plate motion. Consequently we define the deformation in the back-arc region ( $v_{\rm backarc}$ ) as the difference between the trench motion and the upper plate motion:

 $v_{\text{backarc}} = v_{\text{trench}} - v_{\text{upper}}$ 

A positive  $v_{\rm backarc}$  represents extension (including any amount of back-arc spreading) and a negative quantity represents the rate of compression or shortening. These simple kinematic relations can be divided separated into an oscillatory component (in one or both of the upper plate and trench motions) and a translational component (based on the speed at which the trench is retreating) upon which is the oscillatory component is superimposed.

Hyper-episodicity will arise if  $v_{\rm backarc}$  shifts back and forth between positive and negative values. Typically, this would be accomplished when the upper plate motion is approximately constant (in the direction of retreat) and the magnitude of the trench oscillations is larger. However, it is conceivable to have a relatively constant retreating trench combined with a sudden increase in upper plate motion.

Across the globe today, a number of trenches are advancing—the Izu-Bonin Trench, the Mariana Trench, the Japan Trench, the Java-Sunda Trench and the central portion of the Peru-Chile Trench (the Andes subduction zone). The Izu-Bonin, Mariana and Japan all have established back-arc basins, while the others have documented episodes of spreading, quiescence, compression or a combination of these (Fig. 16). The combination of advancing and retreating trench motion places these subduction zones in the category of hyper-episodicity.

Identifying the motion of the trench in the past can be difficult, particularly in the absence of back-arc basin spreading. One example of this is identifying hyper-episodicity in the Solomon Sea, since only a small portion of it is now preserved and our knowledge of its tectonic history is sketchy. However, the Solomon Sea area has been affected by sudden changes in upper (Australian) plate motion rate and direction in the Eocene (Whittaker et al., 2007), leading to the replacement of an extension back-arc spreading regime with compression and subduction of Solomon Sea crust, most of which has now vanished (Gaina and Müller, 2007).

Quasi-episodicity will arise from similar combinations of upper plate and trench motions but shifted towards slightly faster retreating trenches such that  $v_{\rm backarc}$  is always positive with occasional reductions to zero. When such a minimum is attained, rather than a compressional event occurring as in the hyper-episodic case, it is simply expressed as quiescence in tectonic activity. Many such cases are shown in Fig. 16, and this is the dominant form of trench evolution.

Finally, in systems which have the greatest amount of trench retreat, combinations of upper plate and trench motions are always positive leading to continuous extension or back-arc spreading. In this case, there is no episodicity in the system but episodicity may be apparent when a ridge jump is misinterpreted or lack of data exists for some time period. This is to do with upper plate strength and yielding, rather than the dynamics of the trench itself and so we term this pseudo-episodicity. Such is the case with the spreading in the Scotia Sea and extension in the Tyrrhenian Sea and Liguro-Provençal. The complicated pattern of spreading in these regions has caused them to be labelled episodic in nature, but this is most

likely caused by ridge-jumps and we would therefore classify this back-arc as pseudo-episodic.

These three types of episodicity found in nature therefore correspond well to the three types of boundary conditions imposed on the tail of the subducting plate. This boundary condition controls the magnitude of trench retreat velocities from slowest to fastest in the order of pushed, free and fixed. Thus, based on results of our numerical models, the translational component dominates over the oscillatory component in generating the different classes of episodicity. Hyper-episodicity is only observed in models which have an imposed plate velocity and can have an advancing trench. The models with a free-trailing edge exhibit quasi-episodicity as they have trench migration ranging from slowly retreating to stationary. Finally, fixed edge models only have trenches which retreat, and would therefore only correspond to pseudo-episodicity.

The cause of quasi-episodicity in our models is slab-transition zone interactions. In contrast to the pushed models, if a moderate amount of ridge push is balanced by slab pull, the system will tend towards having a trench that is nearly stationary with respect to the mantle. In this situation, as the subducted slab reaches the viscosity increase atop the lower mantle, it undergoes a folding instability. This results in a series of one or more recumbent folds of slab material, each of which expresses itself at the surface as an oscillation in trench migration. We observe a strong correlation in our numerical models between periods of quasi-episodic behaviour on the surface in back-arc regions and piling up of slab material in the transition zone. The timing of the interaction (and the angle of the slab's approach) is determined by a suite of conditions for the subduction system, such as rollback velocity, strength of the slab, strength of mantle's radial viscosity stratification, effect of transition zone phase transitions including any slab detachment through the 670 km discontinuity.

In contrast, hyper-episodicity in our numerical models cannot be caused by slab-transition zone interactions as each of the models experience trench advance initially, meaning the slab is laid out in reverse on the transition zone. However, as the trench advances, the overriding plate area decreases (Fig. 8), creating a resisting force as the upper plate is pushed against the wall. This retards the motion most strongly at the centre, where overriding plate material cannot push outwards as easily as on the edge of the plate, leading to a concave trench with respect to the overriding plate. As the trench becomes increasingly concave, the more difficult for the overriding plate to be compressed in the centre leading to eventual rollback. Rollback is stopped as the trench narrows and the subducting plate thickens (due to the onset of numerical instabilities), concentrating the push force in the centre of the trench again.

There are several other dynamical sources within the mantle (such as mantle avalanches) or global scale tectonic reconfigurations which can produce local oscillations in a given subduction system. Alternatively, the overriding plate can be influenced by farfield stresses from a variety of possible sources which would also result in a significant increase in upper plate motion. An investigation into these processes would be very interesting but would require much larger computational domains than the regional-scale models we have employed as well as a global set of rigid plates.

We are primarily modelling the overriding plate as oceanic lithosphere, not continental lithosphere, so this limits the application of our models to systems which are ocean–ocean subduction. We do not expect that these models are as applicable to the situation in which oceanic lithosphere is subducting under continental lithosphere. Certainly the nature of plate–mantle coupling adjacent to large continents will provide very different controls on the subduction system and should also be the focus of future work. Similarly,

we do not include the type of sophisticated rheologies necessary to allow back-arc spreading centres to naturally and self-consistently evolve with an accompanying complement of oceanic transform faults. Thus our treatment of back-arc spreading is unable to replicate ridge-jumps and therefore only reproduces pseudo-episodicity in a crude sense as the models exhibit monotonic extension. Additionally, since the back-arc spreading ridges are completely passive as they do not add any gravitational load on the overriding plate, we are unable to diagnose whether compression in the back-arc may arise in the overriding plate from the back-arc spreading centre pushing the arc into the subducting plate. This could lead to simultaneous extension and compression with local region of compression at the arc within an overall system which is in extension.

We note our numerical models do not achieve trench advance in a self-consistent manner (naturally arising from the available forces) but rather from an imposed surface velocity. Additionally, an imposed constant velocity is not equivalent to a constant force, but is likely representing a variable force representing a continuously decreasing net ridge push force. Nevertheless, advancing hinges are observed on Earth based on kinematic reconstructions and thus merits some type of kinematically driven system in order to achieve trench advance.

A more self-consistent treatment for generating trench advance remains an outstanding challenge. Some other features which we have not taken into consideration have also been suggested to lead to episodicity. This includes subduction of buoyant material such as continental crust on the overriding plate or oceanic plateaus on the subducting plate (Martinod et al., 2005; Royden and Husson, 2006; van Hunen et al., 2000). Either of these could cause a temporary imbalance between the net slab pull and net ridge push forces and have a significant expression in trench motion.

In addition, it remains an outstanding problem to include the results of research on the mantle wedge (c.f. Arcay et al., 2005) into dynamically self-consistent models at the subduction trench scale, as we have used in this paper. While we have included a weakened mantle wedge in thermo-mechanical numerical models with prescribed plate velocities and ages (Clark and Müller, in press) and a weak-zone in the models in this paper, it remains a challenge to develop a more sophisticated treatment of the mantle wedge in 3D. Furthermore, the global mantle flow has been neglected in regional subduction models and this may prove to play an important role in further understanding of the episodicity of trench movements and back-arc basin formation.

# Acknowledgements

The authors would like to thank Claudio Faccenna and Diane Arcay for their constructive reviews. Funding was provided for this research from an industry linkage grant between the University of Sydney and Exxon Mobil. The authors also acknowledge StatoilHydro's financial support during the publication process.

### References

- Arcay, D., Tric, E., Doin, M.-P., 2005. Numerical simulations of subduction zones: effect of slab dehydration on the mantle wedge dynamics. Phys. Earth Planet. Inter 149
- Bellahsen, N., Faccenna, C., Funiciello, F., 2005. Dynamics of subduction and plate motion in laboratory experiments: insights into the "plate tectonics" behavior of the Earth. J. Geophys. Res. 110, B01401.1–B01401.1.15.
- Buiter, S.J.H., Govers, R., Wortel, M.J.R., 2001. A modelling study of vertical surface displacements at covergent plate margins. Geophys. J. Int. 147, 415–427.
- Bunge, H.-P., Richards, M.A., Baumgardner, J.R., 1997. A sensitivity study of three-dimensional spherical mantle convection at 10<sup>8</sup> Rayleigh number: effects of depth-dependent viscosity, heating mode, and an endothermic phase change. J. Geophys. Res. 102, 11,991–12,007.
- Christensen, U.R., 1996. The influence of trench migration on slab penetration into the lower mantle. Earth Planet. Sci. Lett. 140, 27–39.

- Clark, S.R., Müller, R.D., in press. Convection models in the kamchatka region using imposed plate motion and thermal histories. J. Geodyn., 45.
- Deschamps, A., Lallemand, S., 2002. The West Philippine basin: an Eocene to early Oligocene back arc basin opened between two opposed subduction zones. J. Geophys. Res. 107, EPM 1-1–EPM 1-24.
- Dvorkin, J., Nur, A., Mavko, G., Ben, A.Z., 1993. Narrow subducting slabs and the origin of backarc basins. Tectonophysics 227, 63–79.
- Enns, A., Becker, T.W., Schmeling, H., 2005. The dynamics of subduction and trench migration for viscosity stratification. Geophys. J. Int. 160, 761–775.
- Faccenna, C., Davy, P., Brun, J.-P., Funiciello, R., Giardini, D., Mattei, M., Nalpas, T., 1996. The dynamics of back-arc extension: an experimental approach to the opening of the Tyrrhenian Sea. Geophys. J. Int. 126, 781–795.
- Faccenna, C., Funiciello, F., Giardini, D., Lucente, P., 2001. Episodic back-arc extension during restricted mantle convection in the Central Mediterranean. Earth Planet. Sci. Lett. 187, 105–116.
- Forte, A.M., Peltier, R., 1991. Viscous flow models of global geophysical observables
- 1. Forward problems. J. Geophys. Res. 96, 20131–20159.
  Funiciello, F., Faccenna, C., Giardini, D., Regenauer-Lieb, K., 2003a. Dynamics of retreating slabs: 2 insights from three-dimensional laboratory experiments. J. Geophys. Res. 108, 2207.
- Funiciello, F., Morra, G., Regenauer-Lieb, Giardini, D., 2003b. Dynamics of retreating slabs: 1. Insights from two-dimensional numerical experiments. J. Geophys. Res. 108. ETG11.1–ETG11.17.
- Gaina, C., Müller, D., 2007. Cenozoic tectonic and depth/age evolution of the Indonesian gateway and associated back-arc basins. Earth Sci. Rev. 83, 177–203.
- Garfunkel, Z., Anderson, D.L., Schubert, G., 1986. Mantle curculation and lateral migration of subducting slabs. J. Geophys. Res. 91, 7205–7223.
- Gurnis, M., Mitrovica, J.X., Ritsema, J., van Heijst, H.-J., 2000. Constraining mantle density structure using geological evidence of surface uplift rates: the case of teh African Superplume. Geochem. Geophys. Geosyst., 1.
- Han, L., Gurnis, M., 1999. How valid are dynamic models of subduction and convection when plate motions are prescribed? Phys. Earth Planet. Inter. 110, 235–246.
- Heuret, A., Lallemand, S., 2005. Plate motions, slab dynamics and back-arc deformation. Phys. Earth Planet. Inter. 149, 31–51.
- Jarrad, R.D., 1986. Relations among subduction parameters. Rev. Geophys. 24, 217–284.
- Jolivet, L., Tamaki, K., Fournier, M., 1994. Japan Sea, opening history and mechanism: a synthesis. J. Geophys. Res. 99, 22237–22259.
- Kincaid, C., Olson, P., 1987. An experimental study of subduction and slab migration. J. Geophys. Res. 92, 13832–13840.
- Lallemand, S., Heuret, A., Boutelier, D., 2005. On the relationships between slab dip, back-arc stress, upper plate absolute motion and crustal nature in subduction zones. Eos Trans. AGU 86 (Fall Meet. Suppl.), Abstract T33B-0535.
- Lee, C.-T.A., Chen, W.-P., 2007. Possible density segregation of subducted oceanic lithosphere along a weak serpentinite layer and implications for compositional stratification of the Earth's mantle. Earth Planet. Sci. Lett. 255, 357–366.
- Lister, G.S., Forster, M.A., Rawling, T.J., 2001. Episodicity during orogenesis. In: Miller, J.A., Holdsworth, R.E., Buick, I.S., Hand, M. (Eds.), Continental Reactivation and Reworking, vol. 184 special publication. Geological Society of London, London, pp. 89–113.
- Martinez, F., Fryer, P., Baker, N.A., Yamazaki, T., 1995. Evolution of backarc rifting: Mariana Trough,  $20^\circ-24^\circ$  N. J. Geophys. Res. 100, 3807–3827.
- Martinod, J., Funiciello, F., Labanieh, S., Regard, V., 2005. Dynamical effects of subducting ridges: insights from 3D laboratory models. Geophys. J. Int. 163, 1137–1150.
- Martinod, J., Hatzfeld, D., Brun, J.-P., Davy, P., Gautier, P., 2000. Continental collision, gravity spreading, and kinematics of Aegean and Anatolia. Tectonics 19, 290-299.
- Moresi, L.N., Dufour, F., Mulhaus, H.B., 2003. A lagrangian integration point finite element method for large deformation modeling of viscoelastic geomaterials. J. Comput. Phys. 184, 476–497.
- Morra, G., Regenauer-Lieb, K., 2006. A coupled solid-fluid method for modelling subduction. Philos. Mag. 86, 3307–3323.
- Morra, G., Regenauer-Lieb, K., Giardini, D., 2006. Curvature of oceanic arcs. Geology 34, 877–880.
- Müller, D., Sdrolias, M., Gaina, C., 2006. Reconstructing Vanished Oceans Basins, American Geophysical Union Joint Assembly. American Geophysical Union, Baltimore.
- Regard, V., Faccenna, C., Martinod, J., Bellier, O., 2005. Thermal structure and dynamics of subduction zones: insights from observations and modelling. Phys. Earth Planet. Inter. 149, 99–113.
- Regard, V., Faccenna, C., Martinod, J., Bellier, O., Thomas, J.-C., 2003. From subduction to collision: control of deep processes on the evolution of convergent plate boundary. J. Geophys. Res. 108, ETG 13-1-ETG 13-15.
- Royden, L.H., Husson, L., 2006. Trench motion, slab geometry and viscous stresses in subduction systems. Geophys. J. Int. 167, 881–905.
- Schellart, W.P., 2004. Kinematics of subduction and subduction-induced flow in the upper mantle. J. Geophys. Res. 109, B07401.1–B07401.19.
- Schellart, W.P., Freeman, J., Stegman, D.R., Moresi, L.N., May, D., 2007. Evolution and diversity of subduction zones controlled by slab width. Nature 446, 308– 311.
- Schellart, W.P., Lister, G.S., Jessel, M.W., 2002. Analogue modeling of arc and backarc deformation in the New Hebrides arc and North Fiji Basin. Geology 30, 311–314.

- Sdrolias, M., Müller, R.D., 2006. Controls on back-arc basin formation. Geochem. Geophys. Geosyst. 7, Q04016, doi:10.1029/2005GC001090.
- Sdrolias, M., Roest, W.R., Müller, R.D., 2004. An expression of Philippine plate rotation: the Parece Vela and Shikoku Basins. Tectonophysics 394, 69-86.
- Shemenda, A.I., 1993. Subduction of the lithosphere and back arc dynamics—insights from physical modeling. J. Geophys. Res. 98, 16167–16185. Shemenda, A.I., Groholsky, A.L., 1994. Physical modeling of slow spreading. J. Geo-
- phys. Res. 99, 9137-9153.
- Silver, E.A., Rangin, C., 1991. Leg 124 tectonic sythesis. In: Silver, E.A., Rangin, C., von Breymann, M. (Eds.), Proceedings of the Ocean Drilling Program, Scientific Results, vol. 124. College Station, TX.
- Silver, P.G., Russo, R.M., Lithgow-Bertelloni, C., 1998. Coupling of South American and African plate motion and plate deformation. Science 279, 60-63.
- Sobolev, S.V., Babeyko, A.Y., 2005. What drives orogeny in the Andes? Geology 33, 617-620.
- Spadini, G., Podladchikov, Y., 1996. Spacing of consecutive normal faulting in the lithosphere: a dynamic model for rift axis jumping (Tyrrhenian Sea). Earth Planet. Sci. Lett. 144, 21–34.

- Stegman, D.R., Freeman, J., Schellart, W.P., Moresi, L.N., May, D., 2006. Influence of trench width on subduction hinge retreat rates in 3D models of slab rollback.
- Geochem. Geophys. Geosyst., 7.

  Taylor, B., Zellmer, K., Martinez, F., Goodliffe, A., 1996. Sea-floor spreading in the Lau back-arc basin. Earth Planet. Sci. Lett. 144, 35–40.
- van Hunen, J., van den Berg, A.P., Vlaar, N., 2000. A thermo-mechanical model of horizontal subduction below an overriding plate. Earth Planet. Sci. Lett. 182,
- Whittaker, J.M., Müller, R.D., Sdrolias, M., Heine, C., 2007. Sunda-Java trench kinematics, slab window formation and overriding plate deformation since the Cretaceous Earth and Planetary, Sci. Lett. 255, 445-457
- Zellmer, K., Taylor, B., 2001. A three-plate kinematic model for Lau Basin opening. Geochem. Geophys. Geosyst., 2.
- Zhong, S., Gurnis, M., 1995a. Mantle convection with plates and mobile, faulted plate margins. Science 267, 838-843.
- Zhong, S., Gurnis, M., 1995b. Towards a realistic simulation of plate margins in mantle convection. Geophys. Res. Lett. 22, 981-984.